Metrol. Meas. Syst., Vol. 31 (2024), No. 2
DOI: 10.24425/mms.2024.149698

METROLOGY AND MEASUREMENT SYSTEMS
Index 330930, ISSN 0860-8229
www.metrology.wat.edu.pl

FOURIER TRANSFORM USAGE TO ANALYSE DATA OF POLARISATION PLANE ROTATION MEASUREMENT WITH TFBG SENSOR

Grzegorz Koziel[1)], Damian Harasim[2)], Marta Dziuba-Kozieł[1)], Piotr Kisała[2)]

1) *Lublin University of Technology, Department of Computer Science, Nadbystrzycka 36B,20-618 Lublin, Poland* (✉ *g.koziel@pollub.pl*)
2) *Lublin University of Technology, Department of Electronics and Information Technology, Nadbystrzycka 38A,20-618 Lublin, Poland*

Abstract

The paper presents a method of measuring the angle of light polarisation plane rotation. Measurement is done with a tilted fibre Bragg grating (TFBG), with a tilt angle of 7°, and an optical spectrum analyser. Data obtained with the analyser are processed with a fast Fourier transform (FFT) to obtain frequency representation (FFT coefficients). The rotation angle is calculated by comparing such coefficients obtained from the measurement with the ones collected during measurement set calibration. It has been shown that FFT coefficients change in the function of polarisation plane rotation and in the case of some of them, these changes have regular character and can be used to determine rotation. The method shown works in the range of 0−180° of rotation with an average error of 0.076° and a median error of 0.033°. The highest values of errors appear about 0, 45, 90, 135 and 180°, which is caused by flat characteristics of many frequencies for these angles of rotation. The method discussed could find applications in many fields of structure monitoring and maintenance, where rotation or twist could be used as a quality parameter.

Keywords: tilted fibre Bragg grating, polarisation measurement, optical sensors, fibre sensors.

1. Introduction

Optical fibre sensors constitute a group of measurement devices whose development has continued in recent years. They are very successful in various applications such as medical examination [1, 2] or engineering applications[3, 4]. One of the development directions in optical sensing is application of fibre sensors in which periodic structures are an important field. *Fibre Bragg gratings* (FBGs) are characterised by many advantages over the conventional sensors, such as extremely small size, ability to multiplex many sensors in a single fibre or immunity to electromagnetic interference [3, 5]. One of the possible modifications of FBG internal structure is introducing a tilt angle of the grating fringes related to the cross-section plane of the fibre, which leads to inscription of so called *tilted fibre Bragg gratings* (TFBGs). Tilted gratings have an ability to reflect the light as a coupling of series of cladding modes [6]. The geometrical asymmetry of the TFBG internal structure also leads to obtaining different sensitivities for physical quantities such as surrounding medium refractive index [7, 8], bending [4, 9] or rotation angle of input light polarisation plane.

The rotation of the light polarisation plane can be measured precisely using atomic magnetometers [10], but this is expensive technology. Light polarisation measurement is also possible using the TFBG, which was proved in [11, 12]. Methods [11, 12] rely on measuring the power of light transmitted through a TFBG. The best sensitivity is obtained between 20−70° of rotation. None of these articles determines the method's accuracy. Moreover, the same result will be obtained for angles 90-x degrees and 90+x degrees, where x is a positive number ranging from 0 to 90. In all of these methods, the rotation angle's relation to the transmission coefficient

Article history: received December 2, 2023; revised January 4, 2024; accepted January 22, 2024; available online March 15, 2024.

for the chosen wavelength is used. The interrogation setup could also contain a TFBG followed by FBG [13]. The FBG is to filter the narrow range of wavelengths. Interrogation is done by measuring the power of the reflected signal. The authors examine the method from 0° to 180° of rotation. They indicate that the method can give good results in rotation ranges of 25−65° and 115−155°. For both ranges the method returns the same results, so it is impossible to distinguish in which range the measurement was taken. The authors did not examine method accuracy. In the case of applying TFBGs as physical quantity sensors, polarisation cross-sensitivity could be considered as an interference of measurements. One of the possible solutions to create polarisation-insensitivity is proposed in [14].

The lack of methods that are suitable to work in the full range of rotation was the motivation to create a new method that would offer the possibility of taking measurements in the whole range of rotation. The idea is to treat measurement results obtained from an optical spectrum analyser (OSA) as a signal and process it. Because of this, the following research thesis was put forward: it is possible to measure light polarisation plane rotation in the range from 0°−180°, especially by using additional signal processing methods.

2. **Spectral response of TFBG structure to the changes of input light polarisation angle**

2.1. Measurement setup

For the purpose of measuring polarisation plane rotation, an experimental setup was designed and assembled. The signal from broadband light source S5FC1550S-A2 was directed to the optical lens to create the parallel beam which was transmitted through the polariser to obtain higher polarisation degree. The light was then directed on the half-wave plate THORLABS WPHSM05-1550 which was fixed in the electronically driven rotation stage. Application of the motorised rotator allowed operator to control the rotation angle of the output polarisation plane with 0.1° precision. The beam is coupled by optical lens to the fibre, which is connected to the 1x2 splitter. The reference signal from one of the splitter fibres was used in the measurements presented in the next section. The second fibre was connected to the Ge-doped fibre with a TFBG inscribed. The TFBG used in the examination was a structure with a 7° internal angle, 10mm length inscribed using phase method with BraggStar excimer UV laser. Periodic structure was inscribed by using the phase mask method with excimer BraggStar laser. Signal transmitted through the TFBG was measured by *optical spectrum analyser* (OSA1). The *second optical spectrum analyser* (OSA2) was used to measure spectrum of reference signal. The schematic view of the setup is presented in Fig. 1 in which: 1 – superluminescent diode SLED, 2 – splitter 50:50, 3 – optical lenses, 4 – polariser, 5 – half-wave plate, 6 – optical fibre with TFBG inscribed, 7 – transmission fibre for reference signal, 8 – optical spectrum analyser (OSA1), 9 – optical spectrum analyser for reference spectra measurement (OSA2), 10 – computer. According to the temperature sensitivity of the TFBG, it was mounted in a thermal-stabilised chamber to avoid additional error introduced by temperature changes.

The intrinsic sensitivity of TFBG to changes of the input light polarisation plane angle is based on the geometrical asymmetry of its internal structure. It is necessary to present the orientation of the polarisation plane related to the refractive index periodic zone plane. According to the schematic view of the TFBG fringes presented in Fig. 2, it could be seen that the polarisation state related to the internal structure will repeat at every 180° of the rotation angle.

Metrol. Meas. Syst., Vol. 31 (2024), No. 2
DOI: 10.24425/mms.2024.149698

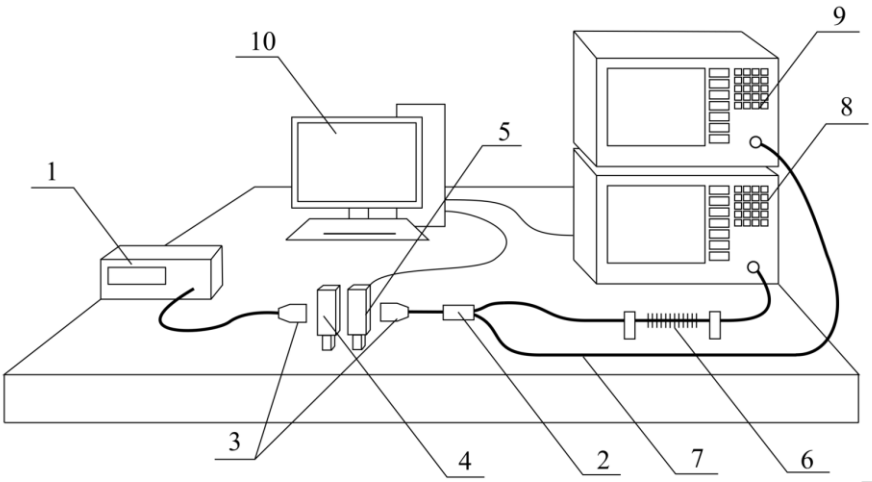

Fig. 1. A scheme of interrogation setup for transmission spectra measurement of 7° TFBG with variable angle of input light polarisation plane, in which: 1 – superluminescent diode SLED, 2 – splitter 50:50, 3 – optical lenses, 4 – polariser, 5 – half-wave plate, 6 – optical fibre with TFBG inscribed, 7 – transmission fibre for reference signal, 8, 9 – optical spectrum analysers, 10 – computer

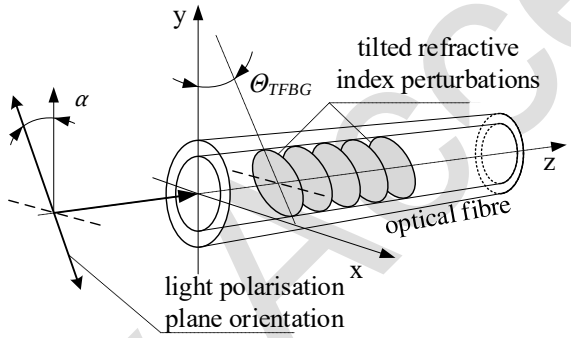

Fig. 2. Schematic view of the input light polarisation plane orientation to TFBG internal structure fringes

2.2. Identification of differences among spectrums obtained with various angles of polarisation

Because of the purpose of the examination, we are interested in finding the part of the spectrum carrying data about light polarisation plane rotation. Identification of these parts was done by comparing spectrums measured for the light after propagating through a fibre with imprinted TFBG for four various angles of input light polarisation plane rotation: 0°, 22°, 45° and 90°. Further in the text, these spectrums will be marked S0, S22, S45, and S90, respectively. The most significant difference exists between S0 and S45 spectrums, as presented in Fig. 3.

Detailed analysis of data obtained from measurement and observation of their changes in the function of polarisation plane rotation allows us to notice that the measured spectrums contain interference in the whole range of wavelengths, but significant changes in the function of rotation can be observed only in some ranges of wavelengths. Because of this, it is important to analyse only this part of the data that carries the significant amount of information about the measured parameter. It reduces the level of interference and shortens the measurement time.

The analysis of obtained results reveals that significant differences between obtained results exist in cladding modes [15] ranging approximately from 1520 nm to 1570 nm. To identify precisely the range of wavelengths that contain the most significant changes caused by the rotation of the input light polarisation plane, an additional analysis was done. The spectrum obtained for rotation of 0° was subtracted from other spectrums considered in this chapter to calculate the differences between them. In each of these differences a maximum value was

found. Next, for each of them the range in which local maxima have values greater or equal to 80% of maximum value was identified. The range beginnings and ends of the obtained analysed spectrum differences were averaged to calculate the beginning and the end of the range to process in further analysis – further called ROI. The range of wavelengths in ROI is 1539 nm – 1559nm. Changes caused by the rotation of input light polarisation are the most significant in this range.

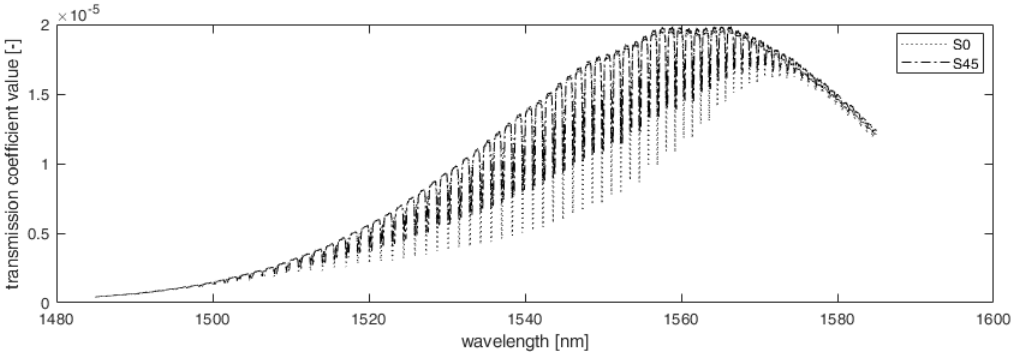

Fig. 3. Spectrums obtained for various angles of light polarisation.

2.3. Measurements with the compensation of half-wave plate influence

The half-wave plate use influences transmitting signal characteristics and can introduce interference to the measured signal. It is caused by a lack of concentricity of the device with adjacent lenses. To examine the influence of the half-wave plate and compensate for it, two independent measurements were taken while examining the interrogation set response to each angle of light polarisation plane rotation. One measurement was taken before a TFBG with OSA2, the other with OSA1 attached to the output of the TFBG. Measurements were taken in the whole examined range of rotation, from 0° to 180°. The values of the power measured behind the TFBG are not aligned with the results presented in [11, 12]. It is caused by the influence of the half-wave plate which has no ideal concentricity. To avoid this influence the measurement results obtained with OSA1 were divided by measurement results obtained with OSA2 for the same angle of rotation. The resulting characteristic is aligned with the results presented in [11, 12]. Thus the influence of the half-wave plate was compensated.

All calculations were done in the Matlab 2023a environment. The measurement result consists of a set of values (samples) representing the power of transmitted light for various wavelengths. For the purpose of the present research, each set of samples obtained in one measurement is treated as a discrete signal.

3. **Digital processing of TFBG polarisation sensor transmission spectrums**

3.1. Fast Fourier Transform

The *Fast Fourier transform* (FFT) is an algorithm that computes the discrete Fourier transform of a sequence of input values[16]. Typically it is used to process signals represented in the time domain to their representation in the frequency domain [17]. This transform is widely used in signal processing, information protection [18, 19], medicine [20, 21], speech processing [22], solving engineering problems[23, 24] and many others. In the case of preparing solutions for embedded devices it is necessary to pay attention to calculations efficiency[25]. A discussion of *non-uniform fast Fourier transform* (NUFFT) usage to process interferograms was presented in [26]. The authors found that NUFFT is comparable to widely used

interpolation in spectral profile shape and spectral noise level but is better in spectral amplitude and computer performance. In [27] the authors present an application of the Fourier transform in Fourier transform holography, which is a lensless imaging technique. The wave is superimposed with the wave scattered by a reference source positioned in the same plane. The Fourier transform is used to reconstruct the distribution of the object from the hologram. The author of [28] proposed a framework based on the Fourier transform, neural networks and other transformations for data analysis. In [29] we find an application of the vehicle-mounted solar occultation flux Fourier transform infrared spectrometer for monitoring air pollution. Fourier transform is used to transform interferograms to obtain infrared absorption spectra. The review of Fourier transform usage shows a big variety of its applications and usability in processing various types of data. Because of this universality, the authors decided to use the FFT transform to process data in the experiment. The Fourier transform is usually calculated using the FFT to save processing time and calculative power. For a discrete signal defined as an ordered sequence of values marked as $x_0, \ldots, x_{n-1}$, the FFT is realised according to the formula 1:

$$X_k = \sum_{m=0}^{n-1} x_m e^{-\frac{i2\pi km}{n}} k = 0, \ldots, n-1 \quad (1),$$

where $e^{i2\pi/n}$ is a primitive *n*-th root of 1.

3.2. Processing idea and sensor calibration

As already mentioned, a signal analysis will be used to extract additional features from measurements obtained with an OSA. At first, a fragment of the data is cropped from a measurement. The fragment contains the measured light power for wavelengths from 1539 to 1559 nm. An example signal after cropping is presented in Fig. 4. In future research, such a fragment of data will be treated as a signal and will be named a “measured signal”.

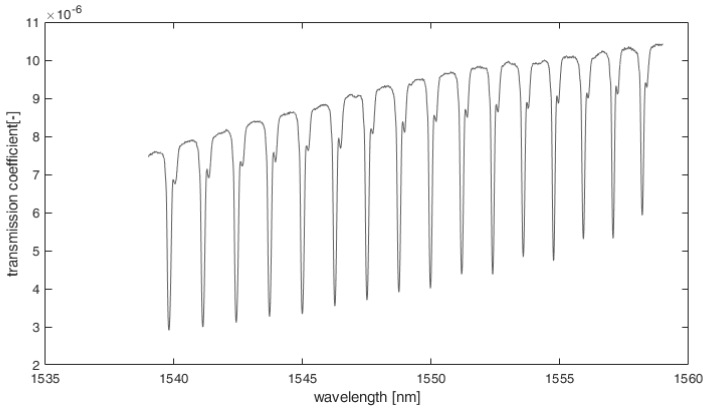

Fig. 4. Cropped measurement result for a rotation equal 0°.

Before further analysis, to minimise the influence of the half-wave plate, compensation is done as presented in Chapter 2.4. The measured signal, after compensation, is transformed to the FFT domain by applying the FFT according to (1). The result is a set of FFT coefficients, representing spectrum frequencies, in the form of complex numbers. These complex numbers are transformed into real numbers by calculating their absolute value. From the resulting set of data, the first half is taken to further analysis. The second half is symmetric, so it can be omitted. Additionally, the first FFT coefficient, carrying information about a constant component, is removed. An example of signal representation after described transformations is presented in Fig. 5.

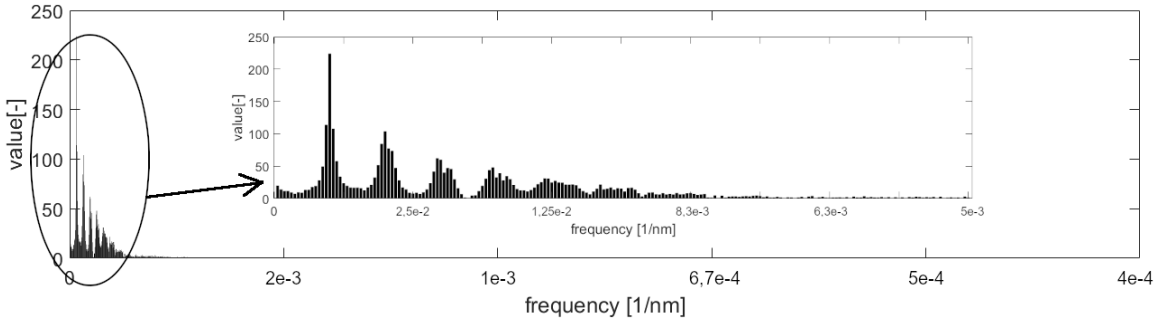

Fig. 5. A FFT domain representation of a signal measured for a rotation equal 0°.

During the calibration process, measurements started from a 0° rotation, were taken with a resolution of 2°, and took 91 measurements finishing with a rotation equal to 180°. After each measurement, the half-wave plate was controlled to change the rotation about 2° clockwise.

Analysis of FFT domain representations obtained for measured signals for various rotations of the polarisation plane allowed us to notice that there are some differences among these representations. These differences are particularly noticeable for frequencies having smaller numbers (1-200). For higher frequencies, it is also possible to observe value changes, but they are usually very random and can be considered to carry a lot of interference. Example FFT domain representations for measurements taken for various angles of rotation are presented in Fig. 6.

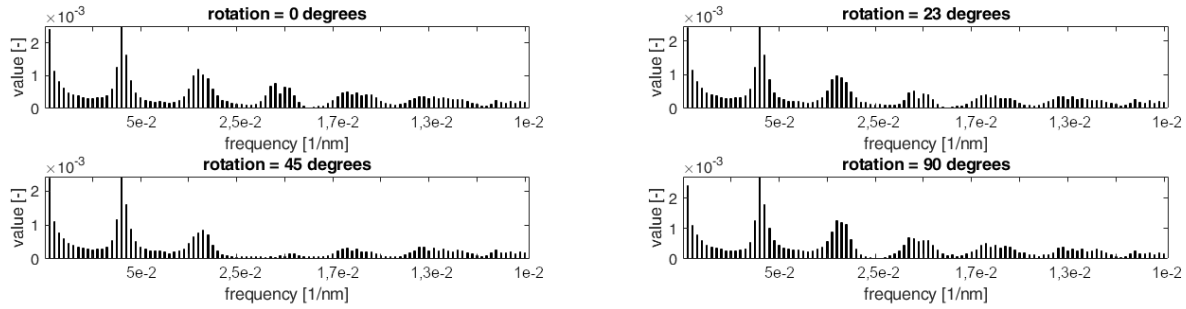

Fig. 6. Example frequency representations of measured signals.

The next step is to identify how the particular frequency changes in the function of light polarisation plane rotation. To achieve this, FFT domain representations of all measurements were recombined, and for each frequency a series of values was created. Each series contained values of the same frequency measured for various angles of polarisation plane rotation. To obtain a continuous function of a given frequency in the function of rotation angle, each pair of adjacent values was connected with a linear function. If we assume that the adjacent values are points P1 and P2 in a flat x, y plane, and their positions are given as coordinates: $P1 = (x_1, y_1)$ and $P2 = (x_2, y_2)$, then the function connecting these points can be described with equation 2:

$$y = \frac{y_2 - y_1}{x_2 - x_1} \cdot \left(x - x_1 \right) + y_1 \tag{2}.$$

A part of the created example function (further called a characteristics) is presented in Fig. 7.

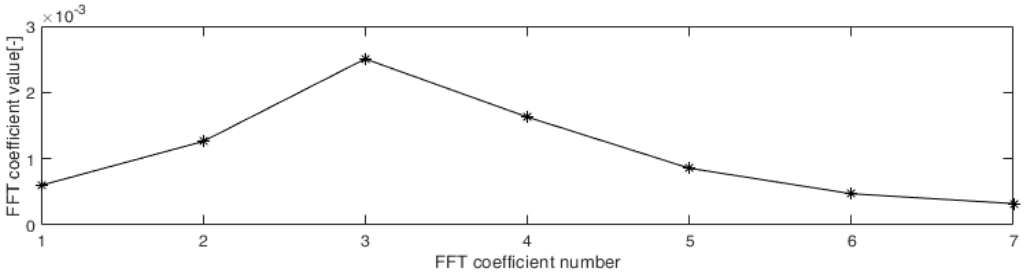

Fig. 7. An example of creating frequency characteristics.

For all frequencies characteristics were made. Their examples are presented in Fig. 8.

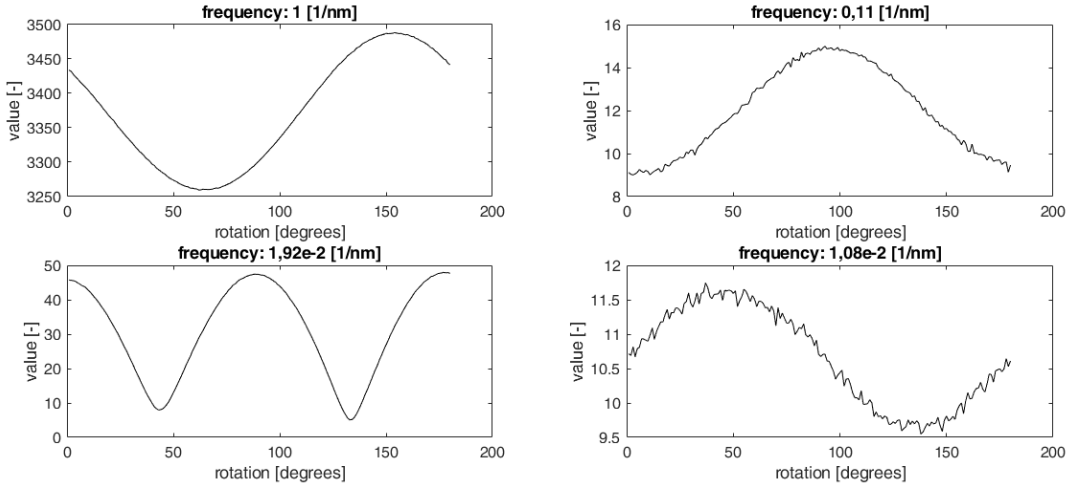

Fig. 8. Characteristics of chosen frequencies.

As can be seen in Fig. 8, the characteristics obtained for various frequencies can vary significantly. They can have various shapes and various levels of interference. An analysis of the characteristics performed revealed that information valuable for our purposes is carried by characteristics of frequencies having numbers lower than 200. The rest of them contain too much noise to be useful. Characteristics of frequencies having numbers smaller than 200 were sorted to choose those that characterise a significant value change in the function of rotation and have a low level of interference. Finally, 36 characteristics were chosen for further processing. In the case of the TFBG used in the experiment, we used characteristics of frequencies: 1, 0,11, 5,56e-2, 3,13e-2 – 2,78e-2, 2,17e-2 – 1,89e-2, 1,75e-2, 1,59e-2, 1,49e-2, 1,47e-2, 1,43e-2, 1,33e-2, 1,3e-2, 1,28e-2, 1,2e-2, 1,18e-2, 1,15e-2, 1,14e-2, 1,1e-2, 1,09e-2, 1,06e-2, 1,05e-2, 1,04e-2, 1,02e-2, 9,43e-3 and 9,26e-3 [1/nm].

Frequencies used may vary depending on the TFBG used. The number of frequencies used should be at least 20. Otherwise, the algorithm may return incorrect readings.

The chosen characteristics and frequencies used to create them are saved permanently. They will be used in the further process of determining an angle of light polarisation plane rotation on the basis of a measurement result. This is the final step of the sensor calibration. The result of calibration is the set of obtained frequency characteristics.

3.3. Measurement idea

When calibration is finished, it is possible to measure a light polarisation plane rotation on the base of measurement taken with an OSA. The result is obtained from measurements processed by calculating absolute values of all obtained frequency coefficients. Next, these

coefficients, being the same frequencies as saved in the sensor calibration process, are examined. The value of the *i*-th frequency coefficient from measurement (FFT_m) is used to determine the light polarisation plane rotation angle that can be read from characteristics of the *i*-th frequency. Such an angle will be further named potential rotation angle and marked with the symbol α_{pot}. If we describe the frequency characteristic as a function:

$$FFTC = f(\alpha) \tag{3},$$

where FFTC is the value of frequency coefficient and α is light polarisation plane rotation angle. α_{pot} are all the values of rotation angle that, when inserted into the equation 3, will give the value FFT_m. It is worth mentioning that, as a result, it is possible to obtain more than one value of α_{pot}, as was presented in the example shown in Fig. 9.

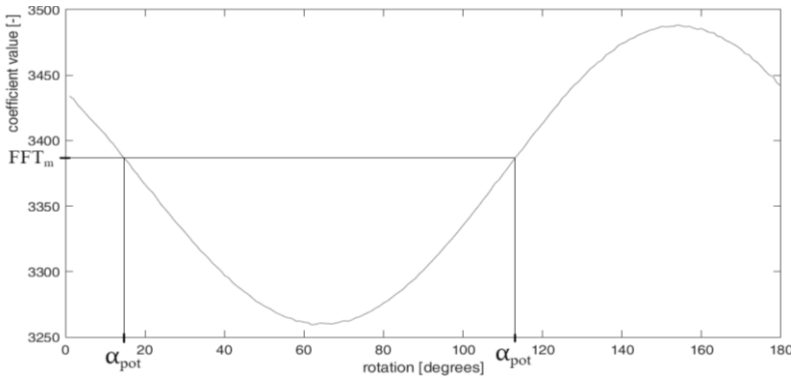

Fig. 9. Determining α_{pot} values on the basis of chosen characteristics.

All characteristics saved during sensor calibration are used to determine α_{pot} values. All α_{pot} values found are saved in a list named PA. After this, values from the list PA are divided into groups. Each group contains $\alpha_{pot} \in <k-0.5, k+0.5)°$, where $k \in Z$ and $k \in \{0,1,2,...,179\}$. Next, the number of α_{pot} in each group is verified. The largest group indicates the light polarisation plane rotation angle. The estimated rotation angle α_{est} is assessed as *k* degrees when the rotation angles from the biggest group $\alpha_{pot} \in <k-0.5, k+0.5)$. That allows us to determine the rotation angle with a precision not lower than ±1.5°. A histogram presenting the results of the measurement done for the rotation angle of 11° is presented in Fig. 10. It can be seen in the histogram that the group of measurements having $\alpha_{pot} \in <10.5,11.5)$ is the largest one. It allows to assess that the angle of rotation was 11°±1.5°.

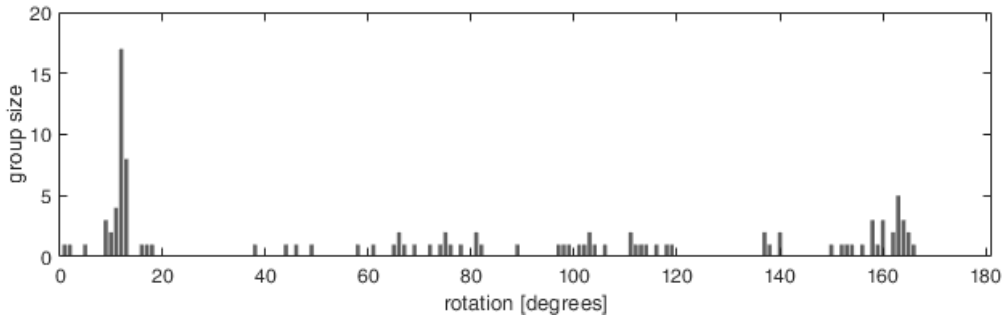

Fig. 10. The histogram obtained for the measurement done for the rotation angle of 11°.

The present method allows a rough estimate of the rotation angle. Inaccuracy was assessed as 1.5°, because in very rare cases the same sizes of groups can appear in two adjacent groups. Then it is impossible to assess which group is the proper one, and the present assessment can

indicate the centre value of the adjacent group as α_{est}. A similar situation can happen when measuring angles close to the boundary of a group (*e.g.* α=1.5).

A rough estimated result needs to be clarified. It is possible by further processing. Among all α_{pot} only these are taken whose meet condition: $|\alpha_{est}- \alpha_{pot}|<2°$. After removing 20% of extreme values from the remaining set (10% of lowest values of angles and 10% of highest ones) the rest of α_{pot} values are used to calculate their average value, which is the final result of measurement. In the present example a measured α=10.96°, so the calculated measurement error in this case is 0,04°. In Fig. 11 a block diagram of invented algorithm is presented.

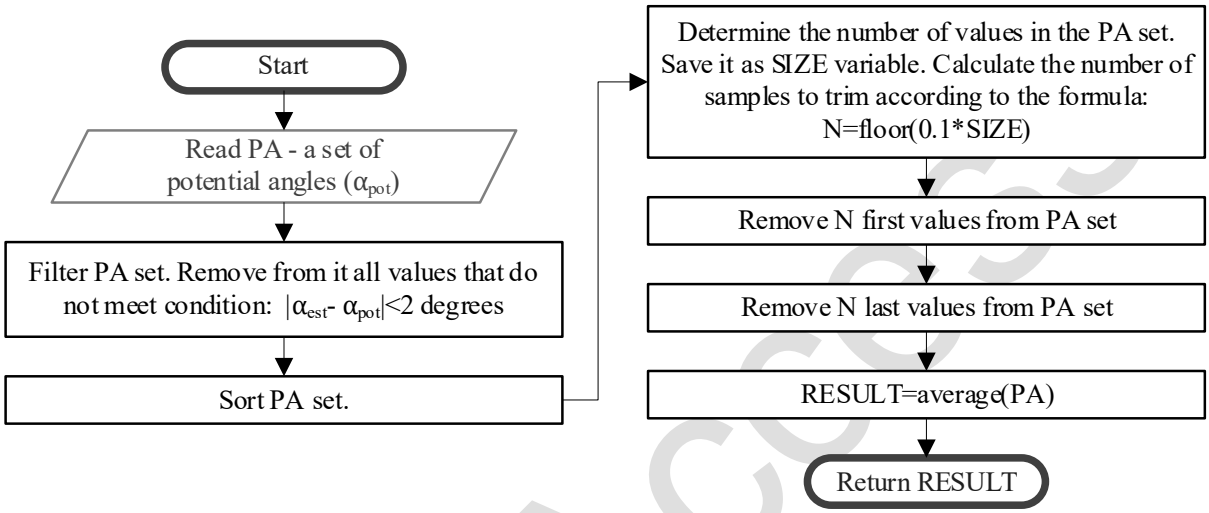

Fig. 11. A diagram of the estimated result clarification algorithm.

4. **Discussion and conclusions**

In the research presented in this paper the proposed polarisation plane rotation sensor was calibrated with a series of measurements taken for angles $\alpha \in \{0,2,4,...,180\}°$. To verify the operation of the sensor a series of measurements were taken for $\alpha \in \{1,3,5,...,179\}°$. Each of these measurements was processed with the proposed algorithm. The obtained results are presented in Fig. 12.

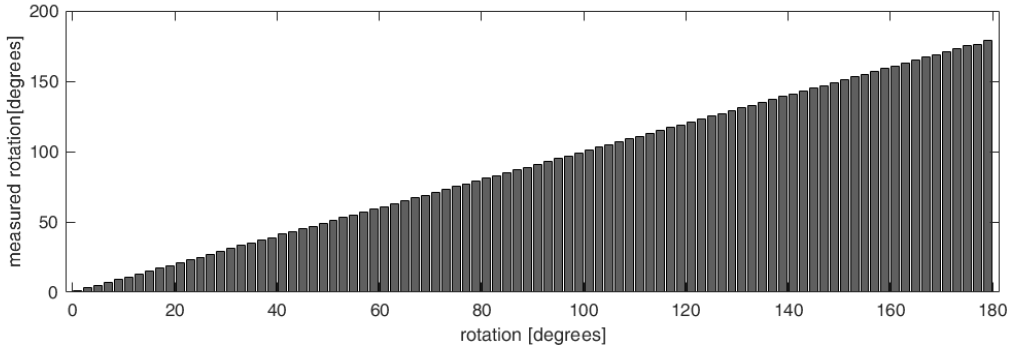

Fig. 12. Sensor verification.

The results presented in Fig. 12 reveal that the proposed method works properly and allows for measuring the angle of rotation in the range 0−180°. To verify the proposed method's accuracy the errors of measurements were calculated. The real rotation of the polarisation plane was known from the half-wave plate setting. For each measurement, this value was subtracted

from the measurement result. Values of errors calculated for all measurements taken during sensor verification are presented on the graph visible in Fig. 13.

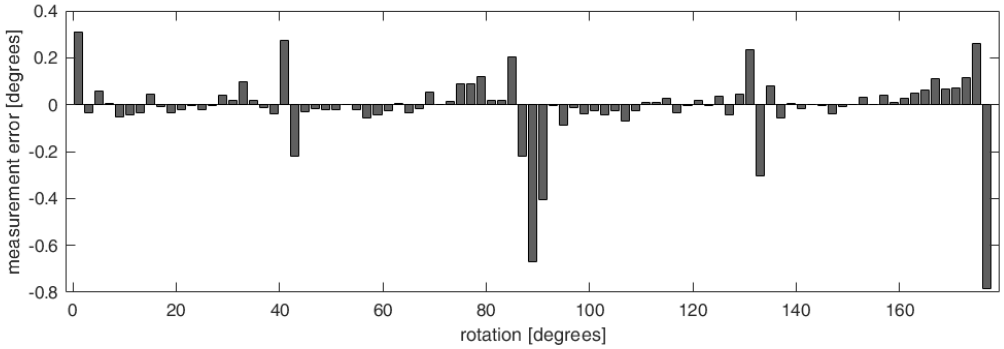

Fig. 13. Measurement errors for various angles.

Analysis of the results presented in Fig. 13 reveals that the proposed method is characterised by bigger inaccuracy close to rotation angles equal 0°, 45°, 90°, 135° and 180°. This is because many of the frequency characteristics have minima or maxima next to these angles (see example characteristics in Fig. 8). A characteristic is flat in its maximum or minimum, which makes the read result more prone to mistakes, especially when some interference appears. Moreover, some characteristics contain a significant level of interference (see characteristic of frequency 1,08e-2 [1/nm] in Fig. 8.) which introduces a significant level of interference to the measurement. This error is smaller in the case of taking a measurement at the angle for which the gradient of the characteristic is big.

Bigger values of errors are found for boundary measurements taken for 1° and 179°. It is noticeable that the error for the measurement taken for 1° rotation is positive and the error for 179° rotation is negative. That can be explained by two phenomena. One is the fact that many frequency characteristics are flat next to these angles of rotation. The second is the way of calculating the rotation angle. To determine the measurement result all values of α_{pot} that meet the condition $|\alpha_{est} - \alpha_{pot}|<2°$ are taken for analysis. In the case of measurements taken for angles smaller than 2° the left boundary of the range from which we can take α_{pot} values is not $|\alpha_{est} - \alpha_{pot}|<2$, but $\alpha_{pot}>0$. Because of the lack of symmetry in the range from which α_{pot} values are taken, there is a bigger chance that a bigger number of α_{pot} values greater than the real angle of rotation will be taken. Finally, an average value of α_{pot} angles from the defined range is calculated, so there is a great chance that the measurement result will be overrated. The same mechanism of error generation exists for angles greater than 178°. For these angles, there is a bigger chance that measurement result will be underrated.

References

[1] Bielecki, Z., Stacewicz, T., Wojtas, J., Mikołajczyk, J., Szabra, D., & Prokopiuk, A. (2018). Selected optoelectronic sensors in medical applications. *Opto-Electronics Review, 26*(2), 122–133. https://doi.org/10.1016/j.opelre.2018.02.007

[2] Prokopiuk, A., Bielecki, Z., & Wojtas, J. (2021). Improving the Accuracy of the Ndir-Based CO_2 Sensor for Breath Analysis. *Metrology and Measurement Systems, 28*(4), 803–812. https://doi.org/10.24425/mms.2021.138578

[3] Tosi, D. (2018). Review of chirped fibre bragg grating (CFBG) fibre-optic sensors and their applications. *Sensors, 18*(7), 2147. https://doi.org/10.3390/s18072147

[4] Kisała, P. (2022). Physical Foundations Determining Spectral Characteristics Measured in Bragg Gratings Subjected to Bending. *Metrology and Measurement Systems, 29*(3), 573–584. https://doi.org/10.24425/mms.2022.142275

[5] Kashyap, R., McKee, P. F., Campbell, R. J., & Williams, D. L. (2014). Novel method of producing all fibre photoinduced chirped gratings. *Electronics Letters, 30*(12), 995–996. https://doi.org/10.1049/el:19940669

[6] Kisała, P., Kalizhanova, A., Kozbakova, A., & Yeraliyeva, B. (2023). Identification of cladding modes in SMF-28 fibres with TFBG structures. *Metrology and Measurement Systems, 30*(3), 507–518. https://doi.org/10.24425/mms.2023.146418

[7] Kisała, P., Mroczka, J., Cięszczyk, S., Skorupski, K., & Panas, P. (2018). Twisted tilted fiber Bragg gratings: New structures and polarization properties. *Optics Letters, 43*(18), 4445–4448. https://doi.org/10.1364/OL.43.004445

[8] Zhou, W., Zhou, Y., & Albert, J. (2017). A true fiber optic refractometer. *Laser & Photonics Review, 11*(1), 1600157. https://doi.org/10.1002/lpor.201600157

[9] Harasim, D. (2021). Temperature-insensitive bending measurement method using optical fiber sensors. *Sensors and Actuators A – Physical, 332*(2), 13207. https://doi.org/10.1016/j.sna.2021.113207

[10] Peng, X., Zhou, Y., Li, L., Xu, Z., Zhou, M., & Xu, X. (2021). High precision measurement of light polarization using a Cs atomic magnetometer configuration. *Journal of Physics B: Atomic, Molecular and Optical Physics, 54,* 105401. https://doi.org/10.1088/1361-6455/abfd03

[11] Harasim, D., & Kusambayeva, N. (2018). The optical measurement method for structural twist monitoring with using tilted Bragg grating sensor. *Przegląd Elektrotechniczny, 94*(7), 62–95. https://doi.org/10.15199/48.2018.07.15

[12] Kisała, P., Skorupski, K., Cięszczyk, S., Panas, P., & Klimek, J. (2018). Rotation and Twist Measurement Using Tilted Fibre Bragg Gratings. *Metrology and Measurement Systems, 25*(3), 429–440. https://doi.org/10.24425/123893

[13] Zheng, J., Dong X., Ji, J., Su, H., & Shum P. P. (2014). Power-referenced refractometer with tilted fiber Bragg grating cascaded by chirped grating. *Optics Communications, 312,* 106–109. https://doi.org/10.1016/j.optcom.2013.09.026

[14] Harasim, D. (2022). Polarization-insensitive refractive index measurement using cascaded perpendicular tilted fiber Bragg gratings. *Measurement, 202,* 111845. doi.org/10.1016/j.measurement.2022.111845

[15] Kisała, P., Kalizhanova, A., Kozbakova, A., & Yeraliyeva, B. (2023). Identification of Cladding Modes in Smf-28 Fibers With TFBG Structures. *Metrology and Measurement Systems, 30*(3), 507–518. https://doi.org/10.24425/mms.2023.146418

[16] Oberst, U. (2007). The Fast Fourier transform. *SIAM Journal on Control and Optimization, 46*(2), 496–540. https://doi.org/10.1137/060658242

[17] Ricaud, B., Borgnat, P., Tremblay, N., Gonçalves, P., & Vandergheynst, P. (2019). Fourier could be a data scientist: From graph Fourier transform to signal processing on graphs. *Comptes Rendus Physique 20*(5), 474–488. https://doi.org/10.1016/j.crhy.2019.08.003

[18] Koziel, G. (2011). Fourier Transform Based Methods in Sound Steganography. *Actual Problems of Economics, 120*, 321–328.

[19] Koziel, G. (2014). Simplified Steganographic Algorithm Based on Fourier Transform. Advanced Science Letters, 20(2), 505–509. https://doi.org/10.1166/asl.2014.5322

[20] Armaselu, A. (2017). New Spectral Applications of the Fourier Transforms in Medicine, Biological and Biomedical Fields. In G. Nikolic, D. Cvetkovic, & M. Cakic (Eds.)., *Fourier Transforms - High-Tech Application and Current Trends* (pp. 235–252). IntechOpen. https://doi.org/10.5772/66577

[21] Bondesson, D., Schneider, MJ., Gaass, T., Kuhn, B., Bauman, G., Dietrich, O., & Dinkel, J. (2019). Nonuniform Fourier-decomposition MRI for ventilation- and perfusion-weighted imaging of the lung. *Magnetic Resonance in Medicine, 82*(4), 1312–1321. https://doi.org/10.1002/mrm.27803

[22] Powroźnik, P., & Czerwiński, D. (2016). Spectral Methods in Polish Emotional Speech Recognition, *Advances in Science and Technology Research Journal, 10*(32), 73–81. https://doi.org/10.12913/22998624/65138

[23] Luo, Z., Peng, Y., Dong, X., & Qian, H. (2023). Rotating machinery fault diagnosis using dimension expansion and Antisym Net lightweight convolutional neural network. *Measurement Science and Technology, 34*(11), 115005. https://doi.org/10.1088/1361-6501/ace928

[24] Zygarlicki, J., & Mroczka, J. (2011). Short Time Algorithm of Power Waveforms Fundamental Harmonic Estimation with Use of Prony's Methods. *Metrology and Measurement Systems, 18*(3), 371–378. https://doi.org/10.2478/v10178-011-0004-z

[25] Zygarlicki, J., Zygarlicka, M., & Mroczka. J. (2020). Fast Four-Point Estimators of Sinusoidal Signal Parameters - Numerical Optimisations for Embedded Measuring Systems. *Metrology and Measurement Systems, 27*(3), 465–472. https://doi.org/10.24425/mms.2020.132782

[26] Wen, M., & Houlihan, J. (2023). Application of the non-uniform Fourier transform to non-uniformly sampled Fourier transform spectrometers. *Optics Communications, 540*, 129491. https://doi.org/10.1016/j.optcom.2023.129491

[27] Mustafi, S., & Latychevskaia, T. (2023). Fourier Transform Holography: A Lensless Imaging Technique, Its Principles and Applications. *Photonics, 10*(2), 153. https://doi.org/10.3390/photonics10020153

[28] Sorvisto, D. (2023). Applications of the discrete-time Fourier transform to data analysis. *International Journal of Data Science and Analytics, 16*(4), 435–440. https://doi.org/10.1007/s41060-023-00409-5

[29] Deng, YS., Xu, L., Sheng, XC., Sun, YF.,; Xu, HY., Xu, HY., & Wu, HT. (2023). Vehicle-Mounted Solar Occultation Flux Fourier Transform Infrared Spectrometer and Its Remote Sensing Application. *Sensors, 23*(9), 4317. https://doi.org/10.3390/s23094317

Grzegorz Kozieł received his Ph.D. degree from Lublin University of Technology, Poland, in 2011. He is currently the Head of the Information Protection and Operating Systems Department at the University. He has authored or coauthored over 80 publications and book chapters, and 1 book.

Piotr Kisała received a diploma in informatics and computer networks from Maria Curie-Skłodowska University, Poland. He received the Ph.D. degree in 2009 and Habilitation degree in 2013 and the title of professor in 2020. He is currently head of Optoelectronic & ICT Department at LUT. His research interests include optical sensor projects, fabrication and testing and the design and development of unconventional FBG sensors. Prof. Kisała has authored over 80 journal publications and conference contributions and 6 patents.

Marta Dziuba-Kozieł was born in Nowa Dęba, Poland in 1978. She received the M.Sc. (2002) degree from University of Maria Skłodowska-Curie (UMCS), Poland and MBA (2008) from University of Illinois. From 2002 to 2023 she has held various positions in business and technology companies. She is currently conducting research in the field of digital signals processing.

Damian Harasim has received PhD degree in Automation, Electronics and Electrical Engineering at the Faculty of Electrical Engineering and Computer Science at AGH Univeristy of Krakow, Poland in 2022. His current research interests lie in fabrication and characterisation of optical sensing systems, especially based on unconventional fiber Bragg grating structures. He is currently employed as assistant professor in Lublin University of Technology, Poland.